Structural and Electronic Properties of Some Metal Oxides Content in Electric-Arc Furnace Dust

Oday H. Ahmed

Department of Physics, College of Education, Al-Iraqia University, Baghdad, IRAQ

Steel manufacturing facilities approximately emit 6Mt of electric-arc furnace dust (EAFD) annually. This dust signifies a major source of recyclable metal oxides. Investigation of those metal oxides properties are beneficial not only for applications in photonics, electronics, sensors and optics, but also for developing new generation devices with a high execution. This work represents a systematic computational investigation to examine the structural and electronic properties of the simple metal oxides content in EAFD then compared to the obtained findings of previous experimental studies. Particularly, carrying out accurate density function theory (DFT) calculations give a detailed atomic-base insight of metal oxides that could not be obtained by merely interpreting experimental results. Simulated results presented herein for the structural and electronic properties correlate very well with experiment values.

Keywords: Electric-arc Furnace Dust, Electronic properties, Metal oxides, Recyclable metals
Received: 21 December 2023; **Revised:** 31 December 2023; **Accepted:** 07 January 2024

1. Introduction

The global production of crude steel throughout electric-arc furnace technology has extraordinarily raised approximately from ~30% to ~40% through the last two decades with a potential schemed grow of another 10% by 2024 [1]. The global formation of electric-arc furnace dust (EAFD) is evaluated to be between 6 to 8 million tons annually [2, 3]. EAFD is a high-volume steel industrial by-products that is harmful to environment and human health [4]. This dust comprises numerous organic toxic materials in addition to various types of elements. EAFD processing is the procedure to make the residue harmless for disposal and to recover the valuable metals [5]. Typically, the principal metals of EAFD are zinc and iron followed by calcium. This is promoted by Pickles who found that the calcium performed the third highest elements in EAFD after iron and zinc [6]. Dust also contains a small but significant amount of considerable economic values of metallic such as nickel, magnesium, manganese, cadmium, copper and lead [7]. Those small amount of metallic are found either in the form of free or mixed oxide structures [8]. Metal oxides can be used in numerous applications due to their multiple optical and electronic such as medical technology, environmental remediation, water treatment, energy, smart sensors, and catalysis with their applications projected to increase with a projected raise for more developing applications [9]. These wide range of applications quite depend on the morphology, physical properties and atomic structure of metal oxides [10]. Among those compounds, simple metal oxides, have attracted interest of both theoretical [11,12] and experimental studies [13,14] by various researchers, who investigated the optical, elastic, structural, electronic, thermodynamic features. Despite of those several previous studies, a detail mechanistic understanding of their characteristic remains not quite demonstrated on a precise atomic scale. This, in turn, will provide an atomic-based insight into structure and electronic properties that might not be easily acquired via just interpreting the experimental measurements. Computational modelling and quantum mechanical simulations throughout utilizing accurate density functional theory (DFT) calculations have had an unique unparalleled influence in providing an intuitive understanding of challenging issues pertinent for the most of the material investigations and experimental designs [15]. DFT is a modelling method that can be applied by numerous field like physics, material science and chemistry to compute the structural and electronic properties at zero points of the energy or at the ground state of the system [16].

Indeed, this contribution reports an inclusive density functional theory (DFT) study into the modelling structural and electronic properties (i.e. lattice constant, X-O band length, band gap energy and band structure) of monovalent metal oxides content in EAFD (namely; calcium oxide, magnesium oxide, nickel oxide, lead oxide and zinc oxide). Moreover, this manuscript displays a comparative research of the structural and electronic properties with experimental investigations for the selected metal oxides.

2. Computational Method

Numerical structural and electronic optimizations presented here were performed within the density functional theory (DFT) framework. All *ab initio* calculations reported in this work were carried out utilizing the commercial program package Materials Studio included DMol^3 module, developed by Accelrys lnc [17,18]. The accuracy and speed of DMol^3 have been achieved by using numerical functions on an atom-centered grid as its atomic basis. The accurate of atomic basis functions are achieved from solving the DFT equations for single atoms [19]. In this work, we used generalized gradient approximation (GGA) along the exchange-correlation of the Padrew and Wang (PAW) functional in all calculations. The Monkhorst–Pack scheme k-point grid taken as 6×6×6 for all calculations with total energy achieves SCF tolerance of 1×10^{-6} Hartree. The tolerances of maximum displacement and maximum force in all geometry optimization operations were established at 5.0×10^{-3} eV/Å and 4×10^{-3} Å, respectively. Polarization functions with a double -polarized numerical basis set of DNP is comprised for all atoms, using global cut-off of 3.6 Å. Final calculated energies were corrected via a dispersion correction term based on the methodology developed by Tkatchenko and Scheffle.

3. Results and Discussion

It is of a prime significance to demonstrate the expected accuracy scale of the adapted theoretical framework versus experimentally measured values from the literature. In this section, we will investigate the structure parameters (mainly, lattice parameters and interatomic distances) and electronic properties (i.e. band gap energy and band structure) for the selected simple metal oxides individually.

The structure properties of each metal oxide (CaO, MgO, NiO, PbO, and ZnO) are listed in tables (1) and (2), which also comprise results of the available experimental investigations. Table (1) contains calculated lattice parameters with other analogous experimental results. It is important to mention that all the obtained values of lattice parameters for bulks CaO, MgO, NiO, PbO, and ZnO are in a good agreement with the listed experimental data. For instance, our values depart from the analogous experimental values that done by Mammone et al [20], Wyckoff [21], Walls et al. [22], Leciejewicz [23], and Klingshirn et al. [24] by only 0.2%, 3.4%, 4.1%, 8.3/14.3% and 2.8/14.2% for CaO, MgO, NiO, PbO, and ZnO, respectively. Despite this great agreement in the results, it is obvious that there are slightly variance between our values and the experimental results listed in table (1). This is because of the GGA underestimation of volume, indicating that the experimental volumes identify to the negative hydrostatic pressure.

Figure (1) depicts side and top view for the optimized structure of all unit cells. The calculated interatomic distances ($d_{x\text{-}O}$) between the cations (X) and anions atom (O) for all the selected metal oxides of this study amount to 2.627 Å, 2.181 Å, 2.166 Å, 2.583 Å and 1.960 Å for CaO, MgO, NiO, PbO, and ZnO, correspondingly. These values estimate agree responsibly well with the analogous experimental data, for example, those of Gualtieri [25]: 2.524 Å for CaO, Chen et al. [26]: 2.104 Å for MgO, Hong et al. [27]: 1.950 Å for NiO, Shannon et al. [28]: 2.673 Å for PbO and Ermoshin and his co-author [29]:1.992 Å for ZnO.

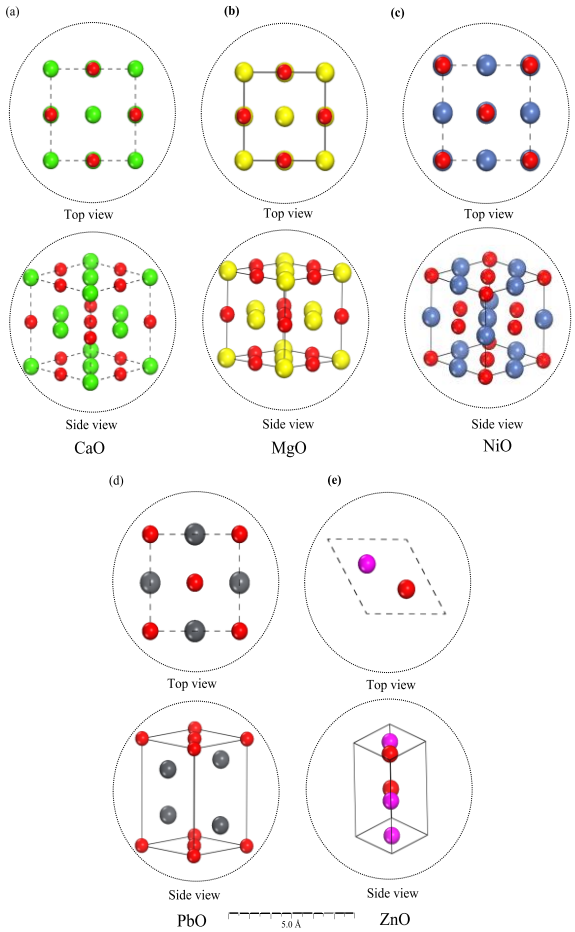

Fig. (1) Top and side view of (a) CaO unit cell, (b) MgO unit cell, (c) NiO unit cell, (d) PbO unit cell and (e) ZnO unit cells. Green, yellow, blue, grey, purple and red spheres signify calcium, magnesium, nickel, lead zinc and oxygen atoms respectively

Table (1) Computed and experimental values of the lattice constant for metal oxides

Metal Oxides	Lattice parameters (Å)		Ref.
	Current work	Experimental	
CaO	$a = b = c = 4.799$	4.810	[20]
MgO	$a = b = c = 4.361$	4.211	[21]
NiO	$a = b = c = 4.332$	4.154	[22]
PbO	$a = b = 4.330$ $c = 5.861$	$a = b = 3.970$ $c = 5.020$	[23]
ZnO	$a = b = 3.343$ $c = 4.461$	$a = b = 3.249$ $c = 5.204$	[24]

Electronic band structure can be known as a critical physical amount that supply a functional

information on the electronic properties and their related characteristic of materials [30]. Figure (2) displays the calculated band structure over different high symmetry lines in the Brillouin zone.

Table (2) Computed and experimental values of the interatomic distance for metal oxide bulks

Metal Oxides	Interatomic distances (Å)		References
	Current work	Experimental	
d_{Ca-O}	2.627	2.524	[25]
d_{Mg-O}	2.181	2.104	[26]
d_{Ni-O}	2.166	1.950	[27]
d_{Pb-O}	2.583	2.673	[28]
d_{Zn-O}	1.960	1.992	[29]

All calculations were done at the calculated equilibrium lattice parameters within GGA (PAW) approximation, as shown in table (1), where there is no spin orbit coupling is contained. From Fig. (2) and table (3), one can summary the following characteristics of the band structures for all metal oxides:

- It is clear that the our obtained results for the band gap energies are in fairly well agreement with previous experimental values from the literature as listed in table (3).
- CaO displays an indirect energy gap with conduction band minimum existing at the X-point as shown in Fig. (2a). The calculated value of band gap energy is 3.04 eV, which underestimates by about 57.18% in reference to experimental value of Whited et al. [30].
- The band structure of MgO are given in Fig. (2b) along the three major high symmetry directions. Two of those three directions display almost the same dispersion in the region around the Γ-point, whereas the third one is more dispersive. As shown in table (3), the calculated band gap energy of MgO is highly underestimated with a value of only 3.7 eV in reference to the experimental value [30].
- NiO produce a band gap energy occurs at a symmetry K-point as shown in Fig. (2c) with a value of 3.53 eV. This value smaller than the experimental values by only 11.75% [31].
- The existence of a narrow band gap in Fig. (2d) demonstrates that PbO is an oxide semiconductor. The conduction band minimum and the valence band maximum are existing in different high symmetry sites, which confirm that this oxide is an indirect band gap semiconductor with band gap energy value of 2.122 eV. The valence band maximum is found at Γ-point, whilst the conduction band minimum is located at the M-point in the Brillouin zones. It is clear from table (3) that the computed band gap energy value closely correspond the reported experimental value, i.e., 1.90 eV [32] with a minor deviations.
- Figure (2e) displays that both of the bottom of the conduction band and the top of the valence band take places at a same symmetry line, i.e., gamma line (Γ). That denotes the direct band gap feature of ZnO. The calculated band gap energy for ZnO is 3.1961 eV, whilst the experimental band gap energy equals to 3.37 eV [33]. So, our calculated band gap underestimated the experimental band gap value with a calculated error of 5.43%. The smaller calculated band gap energy in comparison to the experimental value is because of the inherent drawbacks of theoretical computation.
- The large various between the obtain result and the experimental ones for CaO and MgO are fundamentally owning to the fact that GGA approximation has a simple compose, which is not appropriately flexible for accurately reproducing both its charge derivative as well as the exchange-correlation energy.

Table (3) Computed and experimental values of band gap energy *Eg* (eV) for metal oxide bulks

Metal Oxides	Band gap *Eg* (eV)		References
	Current work	Experimental	
CaO	3.04	7.10	[30]
MgO	4.13	7.83	[30]
NiO	3.53	4.00	[31]
PbO	2.122	1.90	[32]
ZnO	3.19	3.37	[33]

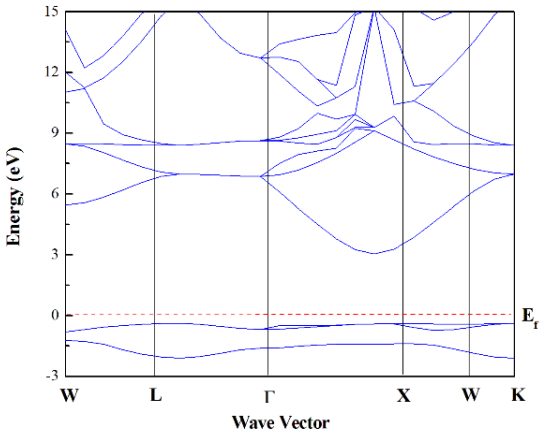

(a) CaO

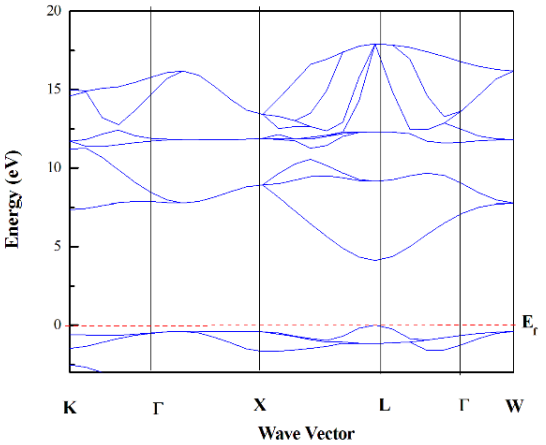

(b) MgO

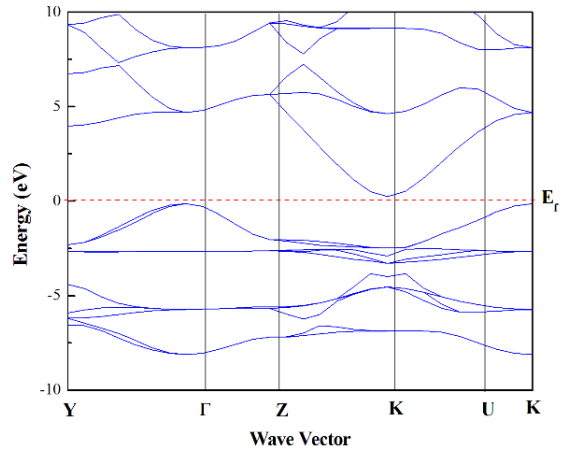

(c) NiO

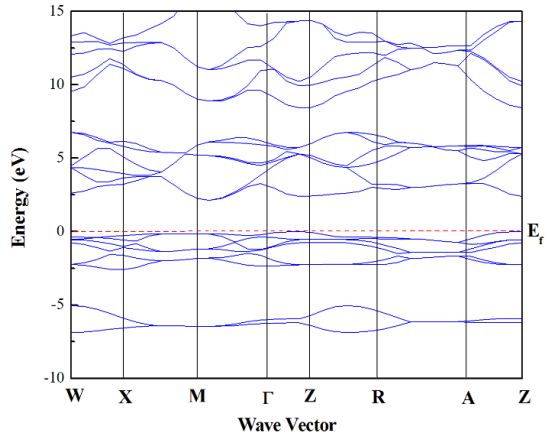

(d) PbO

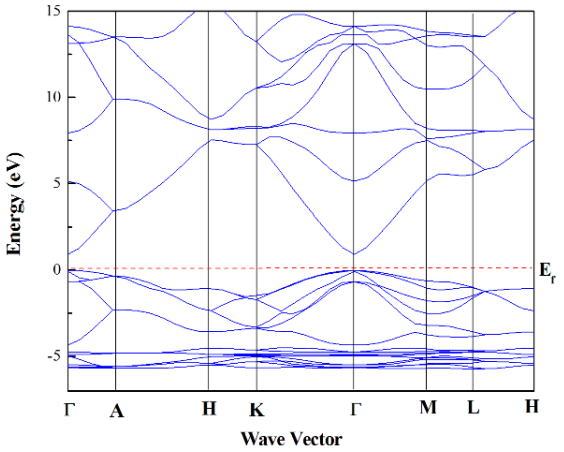

(e) ZnO

Fig. (2) Electronic band structure diagram (a) CaO, (b) MgO, (c) NiO, (d) PbO and (e) ZnO bulks

5. Conclusion

In conclusion, the structural and electronic properties of simple metal oxides included in EAFD systems have been systematically examined via the first principles calculations. Findings suggest that those metal oxides may be promising materials to be applied in developing novel generation devices with a high performance. Subsequently, this contribution can provide significant and beneficial information that can be good guidance for future studies in searching for new multifunctional substances.

References

[1] R.A. Janjua, "Optimisation of electric arc furnace dust recycling and zinc recovery by scrap de-zincing", Ph.D. thesis, Freiberg University of Materials Science and Technology (2008).

[2] J.G.M.S Machado et al., "Chemical, physical, structural and morphological characterization of the electric arc furnace dust", *J. Hazard. Mater.*, 136(3) (2006) 953-960.

[3] N. Leclerc, E. Meux and J.-M. Lecuire, "Hydrometallurgical extraction of zinc from zinc ferrites", *Hydrometal.*, 70(1-3) (2003) 175-183.

[4] A.C. Bayraktar et al., "Stabilization and solidification of electric arc furnace dust originating from steel industry by using low grade MgO", *Arch. Enviro. Protect.*, 41(4) (2015) 62-66.

[5] C.A. Pickles and O. Marzoughi, "Thermodynamic investigation of the sulphation roasting of electric arc furnace dust", *Minerals*, 9(1) (2018) 18.

[6] C.A. Pickles, "Thermodynamic analysis of the selective chlorination of electric arc furnace dust", *J. Hazard. Mater.*, 166(2-3) (2009) 1030-1042.

[7] V. Montenegro et al., "Hydrometallurgical treatment of steelmaking electric arc furnace dusts (EAFD)", *Metallur. Mater. Trans. B*, 44 (2013) 1058-1069.

[8] S. Polsilapa and P. Wangyao, "Glassification of electric arc furnace dust by using fly ash or bagasse ash", *J. Metals Mater. Miner.*, 17(1) (2007) 67-73.

[9] L.-H. Xu, J. Yang and J. Xiao, "Metal oxide nanostructures: synthesis, properties, and applications", *J. Nanotechnol.*, 2015 (2015) 1-2.

[10] M.B. Gawande et al., "Role of mixed metal oxides in catalysis science—versatile applications in organic synthesis", *Catal. Sci. Technol.*, 2(6) (2012) 1113-1125.

[11] R. Pandey and S. Sivaraman, "Spectroscopic properties of defects in alkaline-earth sulfides", *J. Phys. Chem. Solids*, 52(1) (1991) 211-225.

[12] M.M.A. Salam, "Theoretical study of CaO, CaS and CaSe via first-principles calculations", *Results in Phys.*, 10 (2018) 934-945.

[13] A.N. Kravtsova et al., "Electronic structure of M S (M= Ca, Mg, Fe, Mn): X-ray absorption analysis", *Phys. Rev. B*, 69(13) (2004) 134109.

[14] G.A. Saum and E.B. Hensley, "Fundamental optical absorption in the IIA-VIB compounds", *Phys. Rev.*, 113(4) (1959) 1019.

[15] B. Kaduk, T. Kowalczyk and T. van Voorhis, "Constrained density functional theory", *Chem. Rev.*, 112(1) (2012) 321-370.

[16] J.N. Harvey, "On the accuracy of density functional theory in transition metal chemistry", *Ann. Rep. Sec. C Phys. Chem.*, 102 (2006) 203-226.

[17] S.J. Clark et al., "First principles methods using CASTEP", *Zeitschrift für kristallographie-crystalline materials*, 220(5-6) (2005) 567-570.
[18] M. Altarawneh et al., "Co-pyrolysis of polyethylene with products from thermal decomposition of brominated flame retardants", *Chemosph.* 254 (2020) 126766.
[19] B. Delley, "From molecules to solids with the $DMol_3$ approach", *J. Chem. Phys.*, 113(18) (2000) 7756-7764.
[20] J.F. Mammone, H.K. Mao and P.M. Bell, "Equations of state of CaO under static pressure conditions", *Geophys. Res. Lett.*, 8(2) (1981) 140-142.
[21] R.W.G. Wyckoff, "Crystal Structures", vol. 1, Interscience (NY, 1963) 254.
[22] B. Walls et al., "Nanodomain structure of single crystalline nickel oxide", *Sci. Rep.*, 11(1) (2021) 3496.
[23] J. Leciejewicz, "On the crystal structure of tetragonal (red) PbO", *Acta Crystallog.*, 14(12) (1961) 1304-1304.
[24] C.F. Klingshirn et al., "Crystal structure, chemical binding, and lattice properties", in *Zinc Oxide: From Fundamental Properties Towards Novel Applications* (2010) 7-37.
[25] A.F. Gualtieri et al., "Structural and spectroscopic characterization of anorthite synthesized from secondary raw materials", *Period. di Mineral.*, 80(2) (2011) 231-245.
[26] M. Chen et al., "Structures and stabilities of (MgO) n nanoclusters", *J. Phys. Chem. A*, 118(17) (2014) 3136-3146.
[27] J. Hong et al., "H_2O absorption assisted Sr-segregation in strontium nickel oxide based chromium getter and encapsulation with $SrCO_3$", *J. Electrochem. Soc.*, 166(2) (2019) F59.
[28] R.D. Shannon and C. Calvo, "Refinement of the crystal structure of synthetic chervetite, $Pb_2V_2O_7$", *Canadian J. Chem.*, 51(1) (1973) 70-76.
[29] V.A. Ermoshin and V.A. Veryazov, "Electronic Structure Investigation of Bulk ZnO and its (1010) Surface", *phys. stat. sol. b*, 189(2) (1995) K49-K53.
[30] R.C. Whited, C.J. Flaten and W.C. Walker, "Exciton thermoreflectance of MgO and CaO", *Solid State Commun.*, 13(11) (1973) 1903-1905.
[31] H. Villarraga Gomes, "Magneto-optical studies of cobalt-doped nickel oxide thin films", Ph.D. thesis, The University of Puerto Rico (2010).
[32] F.T. Geldasa et al., "Density functional theory study of different metal dopants influence on the structural and electronic properties of a tetragonal α-PbO", *AIP Adv.*, 12(11) (2022) 115302-1-14.
[33] S. Panigrahi, S. Sarkar and D. Basak, "Metal-free doping process to enhance the conductivity of zinc oxide nanorods retaining the transparency", *ACS Appl. Mater. Interfaces*, 4(5) (2012) 2709-2716.

